

Figure 1. Computational domain geometry employed for our DNS studies. The domain is inclined along the phase surfaces of the initial GW, the z' dimension is chosen to be one wavelength, $\lambda = 2\pi/|\mathbf{k}|$, where $\mathbf{k} = (k, l, m)$ is the wavenumber of the initial GW, and the (x', y', z') dimensions have ratios of (3.4, 2.22, 1).

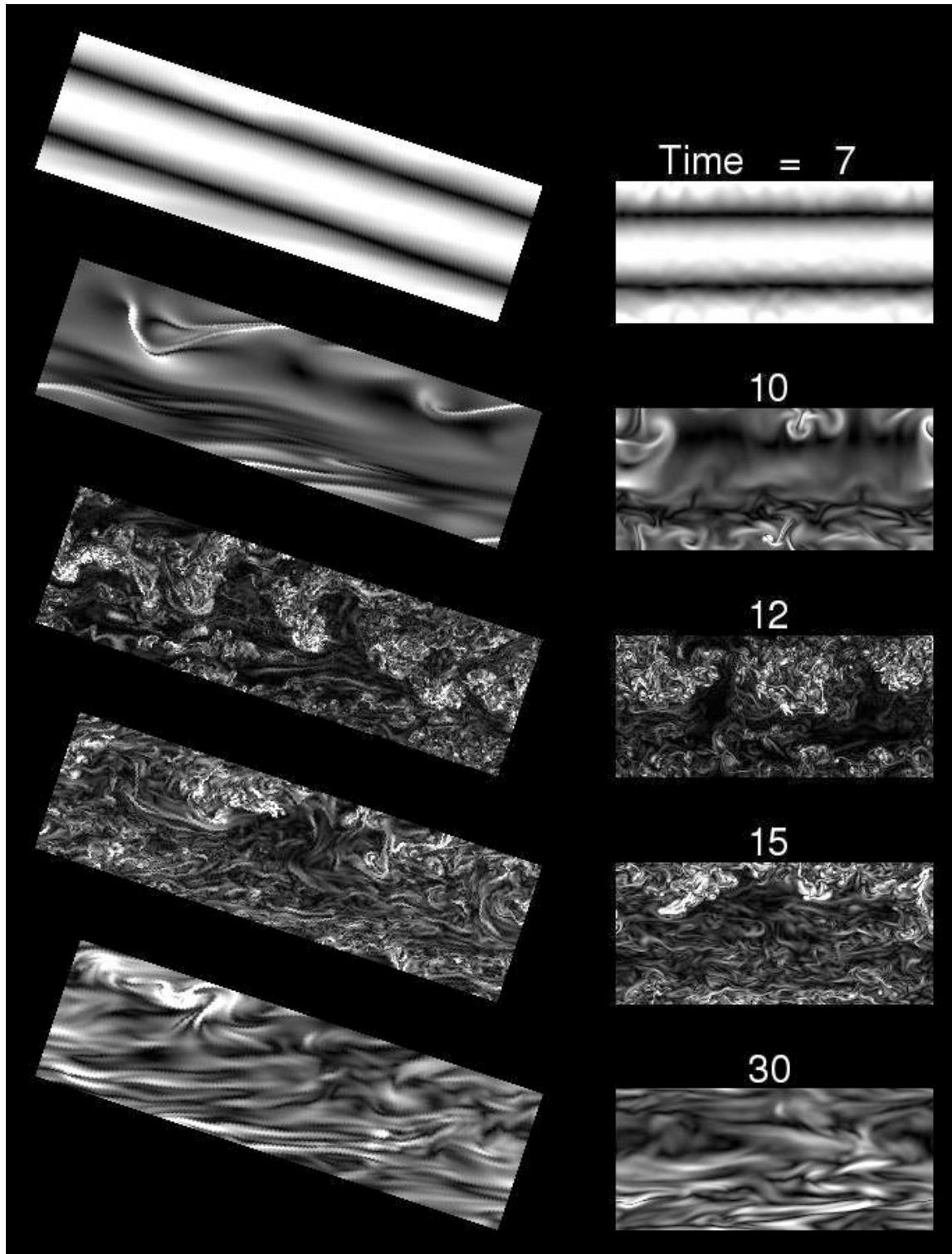


Figure 2. 2D streamwise-vertical (left) and spanwise-vertical (right) cross sections of the wave breaking evolution in vorticity magnitude (white is high, black is zero) for $a = 1.1$ at times of 7, 10, 12, 15, and 30 (in units of T_b). All images are shown with the same GW phase, with the upward motion within the wave field $\frac{1}{4}$ of the domain depth from the top.

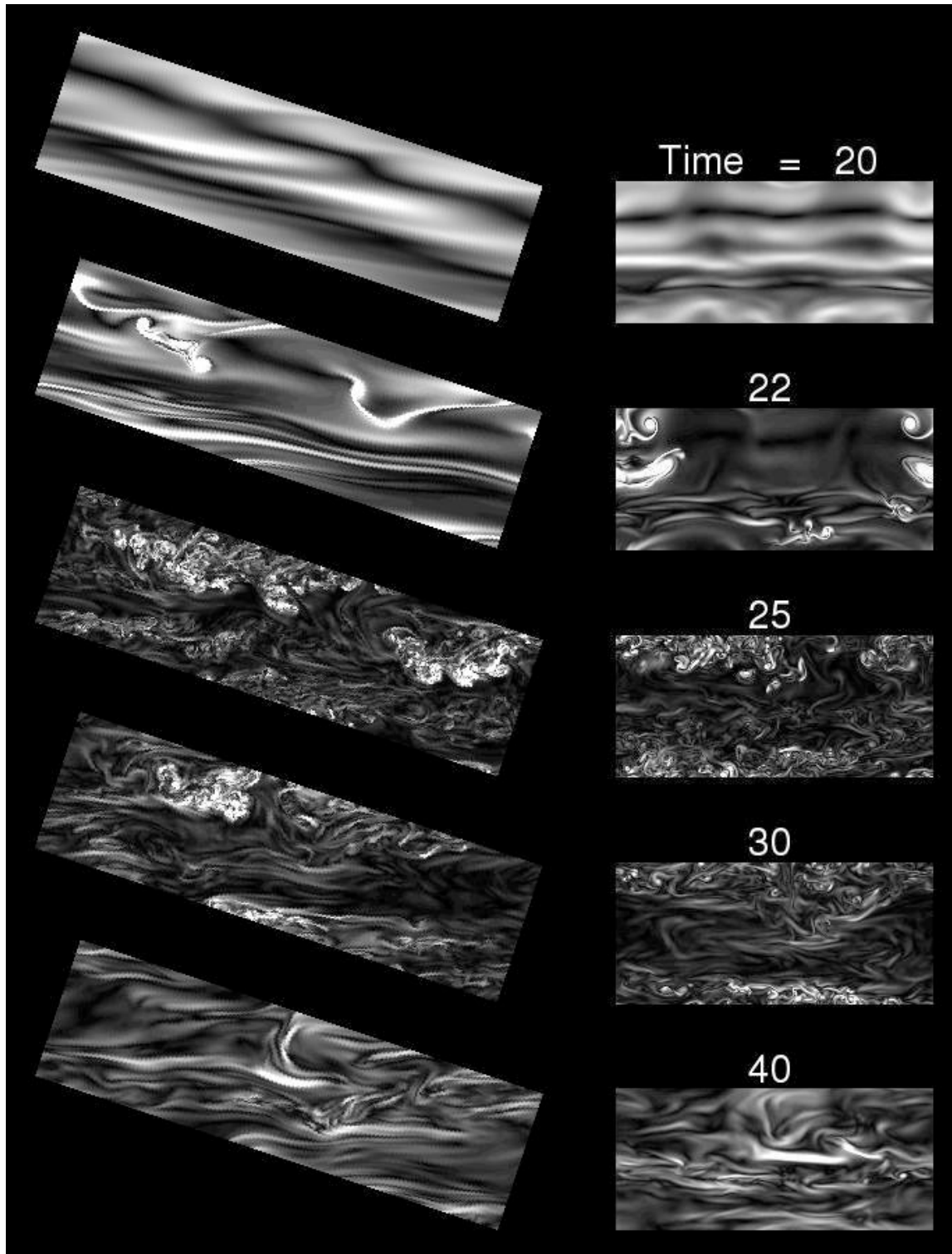


Figure 3. As in Fig. 2, but for $a = 0.9$ at times of 20, 22, 25, 30, and 40 (in units of T_b). Note here that wave breaking begins $\sim 12 T_b$ later than at $a = 1.1$.

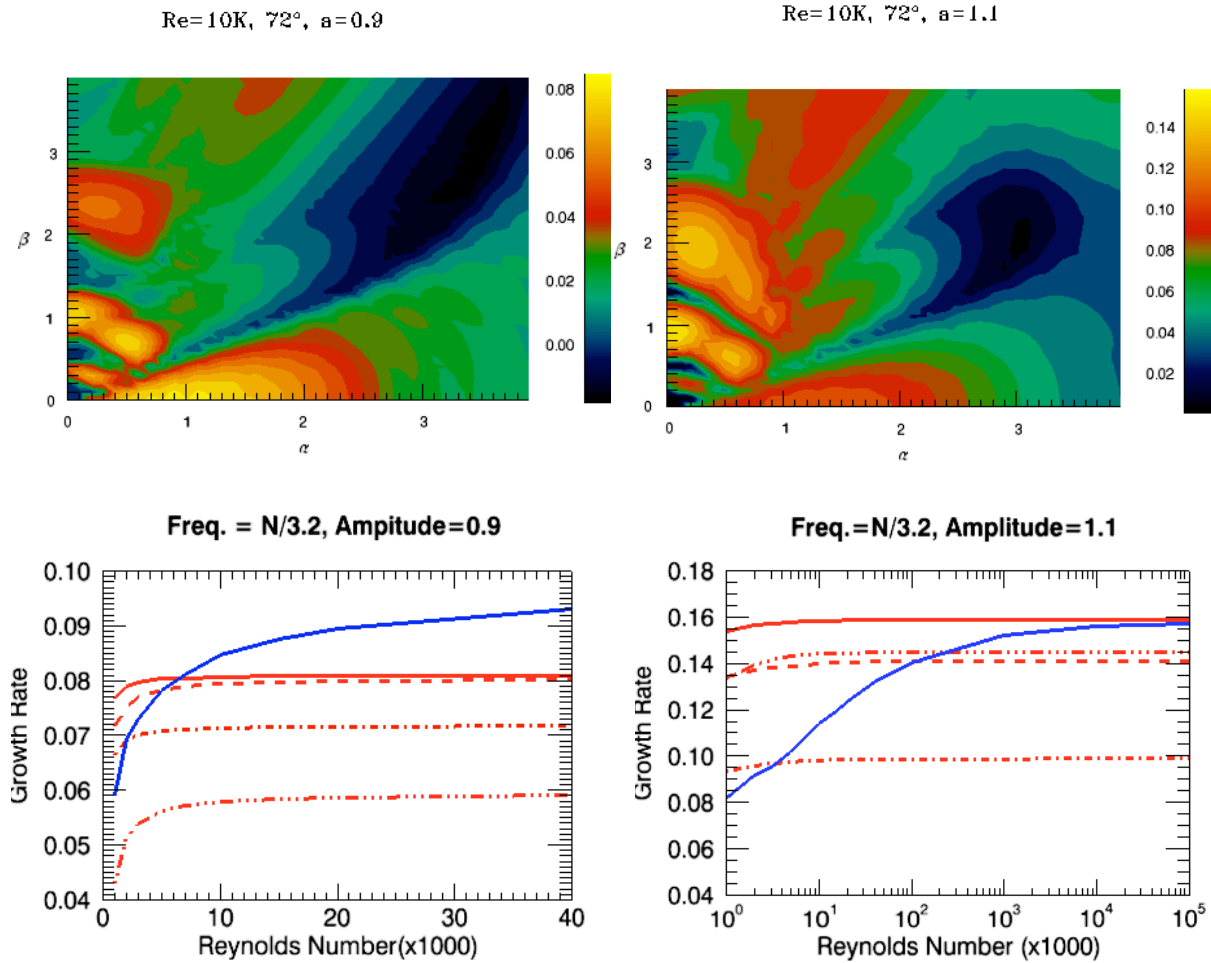


Figure 4. Anticipated modes of instability employing the analysis of Lombard and Riley (1996) for $\omega = N/3.2$, $\text{Re} = 10^4$, and $a = 0.9$ and 1.1 (upper left and right, respectively). Streamwise (α_i) and spanwise (β_i) instability wavenumbers are normalized by the total wavenumber of the initial GW. Maximum growth rates for the dominant 2D ($\beta_i = 0$, blue) and 3D ($\beta_i \neq 0$, solid red) modes for $a = 0.9$ and 1.1 (lower left and right, respectively). Weaker 3D modes are denoted by other dashed and dash-dotted red lines.

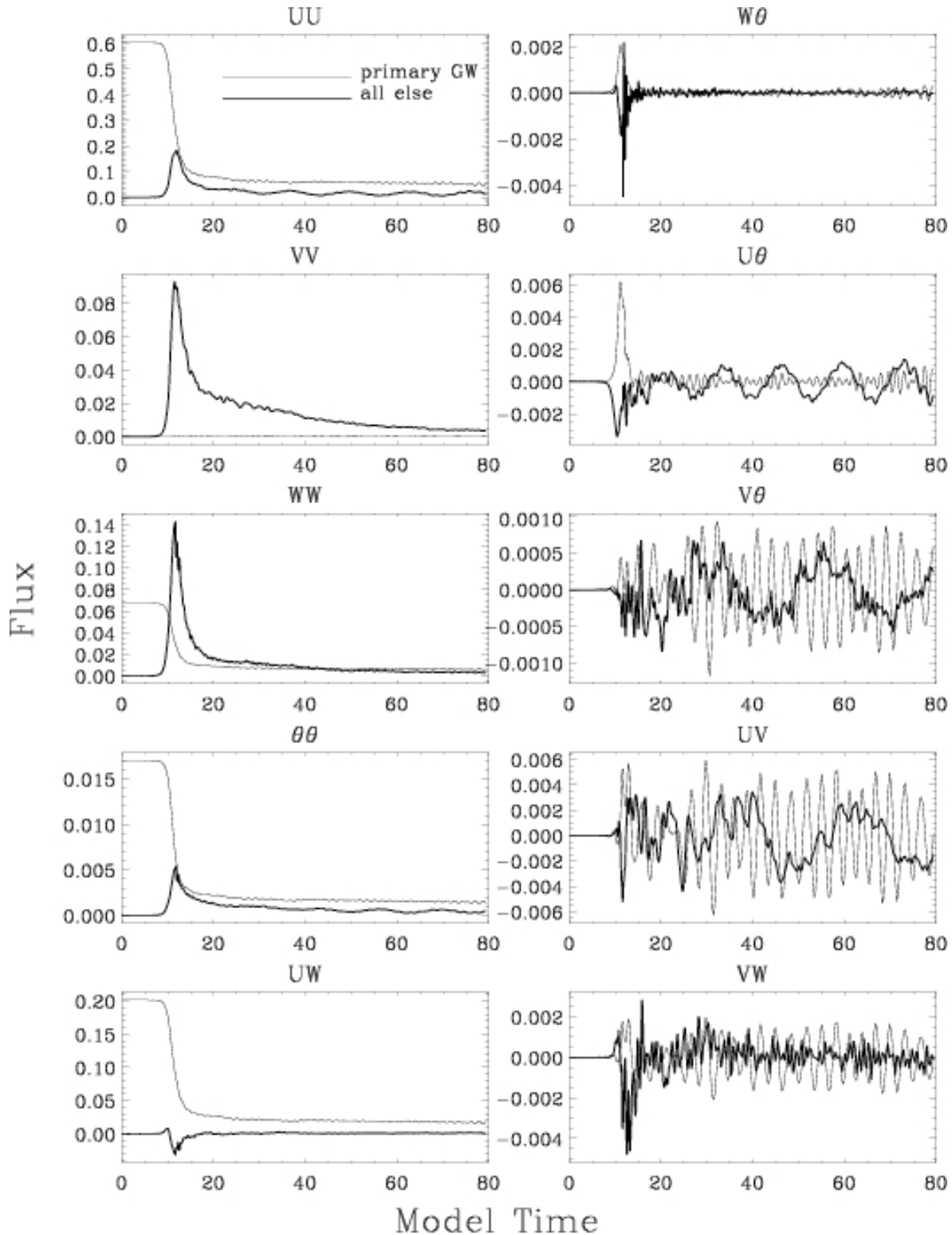


Figure 5. Evolutions of domain-averaged variances of velocities (u , v , w) and normalized potential temperature (θ) (upper four left panels) and covariances (bottom left and right panels) for $a = 1.1$. The primary GW with wavenumber $(0, 0, -1)$ is shown with light lines and all other 2D ($k, l = 0, m$) and 3D ($k, l \neq 0, m$) are shown with heavy lines. Normalized wavenumbers are relative to the component domain dimension.

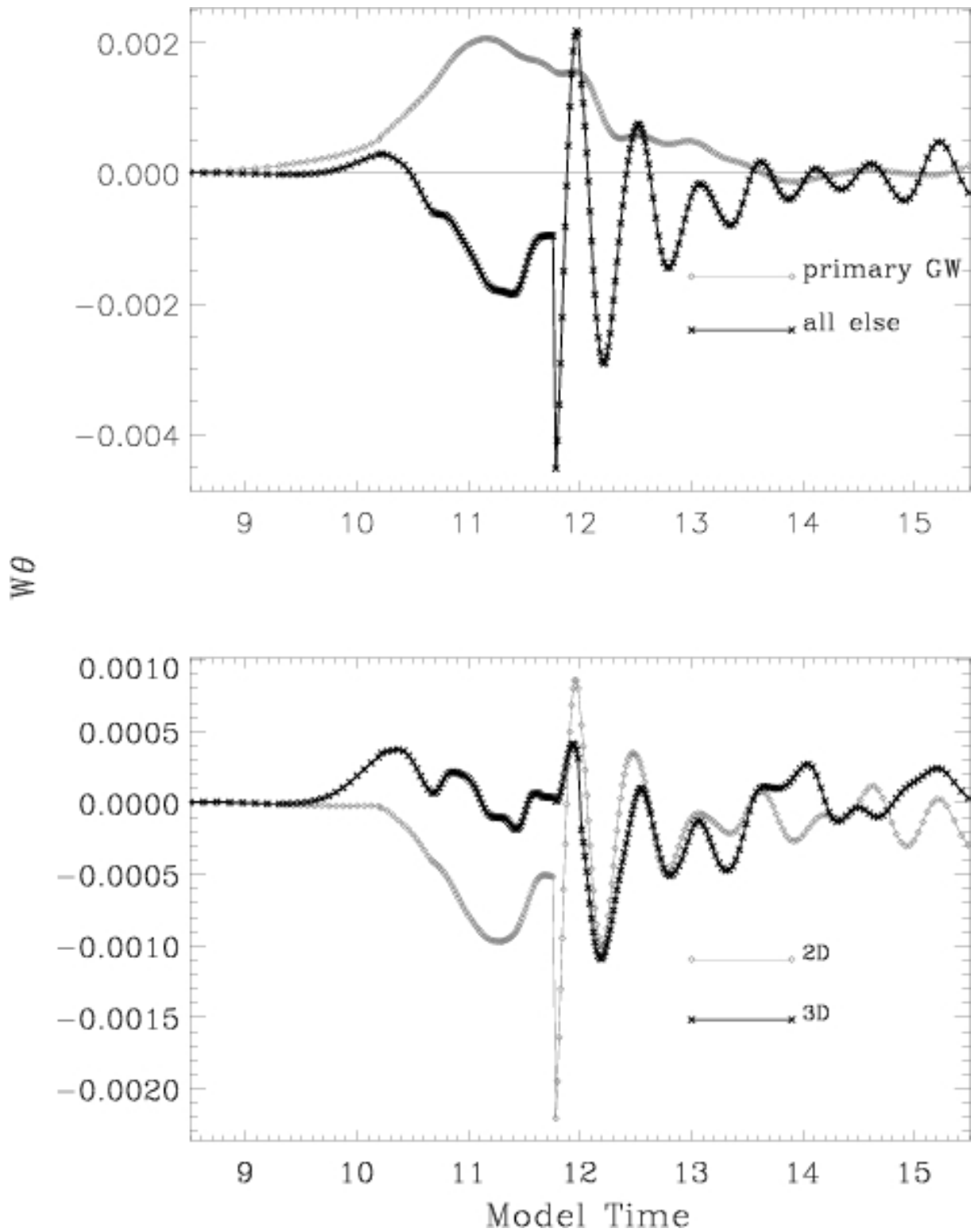


Figure 6. Vertical fluxes of potential temperature for the primary GW and all other motions (top) and for all 2D motions except the primary GW and all 3D motions (bottom) during the interval of strong wave breaking. In the upper (lower) panel, the primary GW (2D) flux is shown with light diamonds and the flux due to all other (3D) motions with dark "x"s.

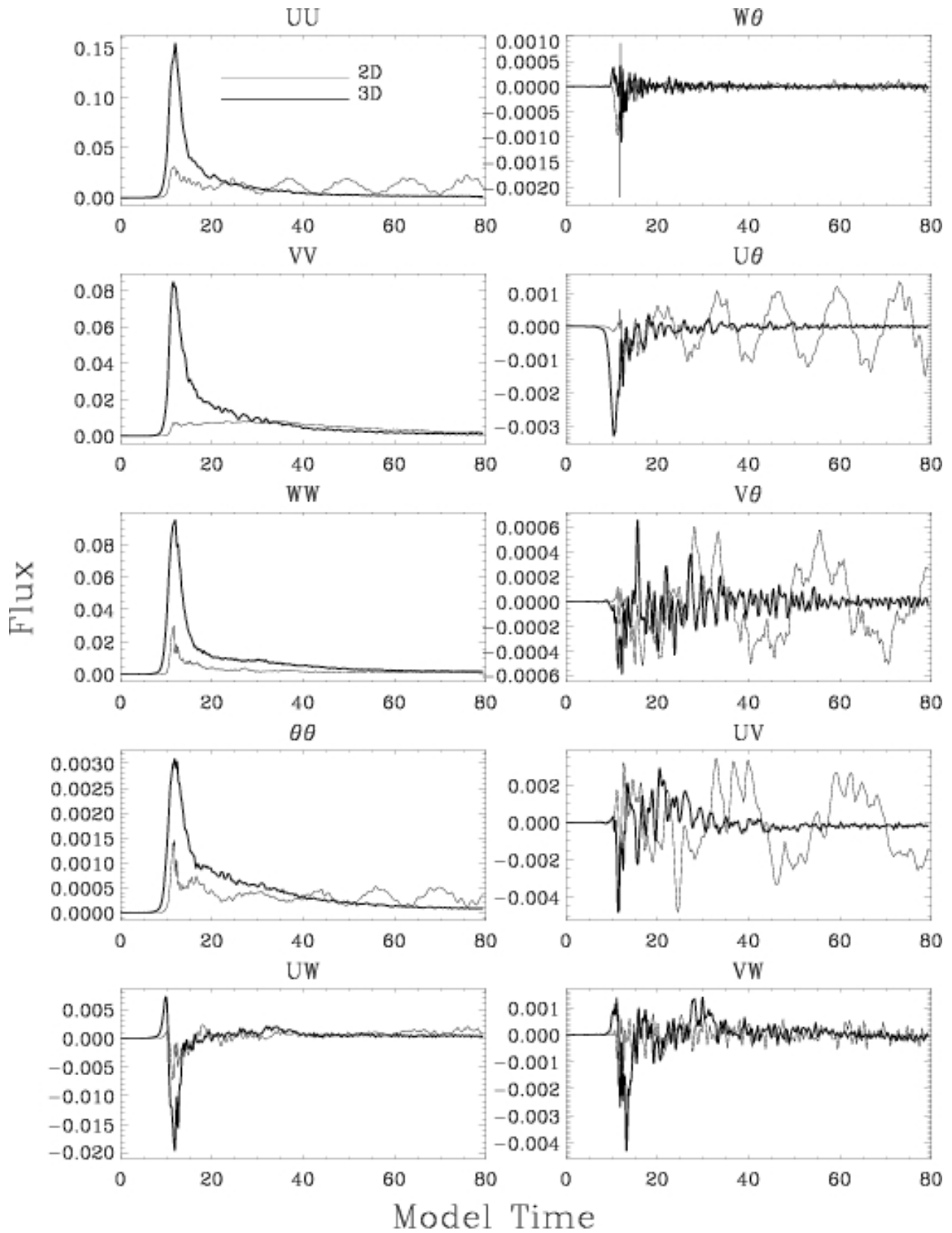


Figure 7. As in Figure 5, but for all 2D motions ($k, l = 0, m$) except $(0, 0, -1)$ (light) and all 3D ($k, l \neq 0, m$) (heavy).

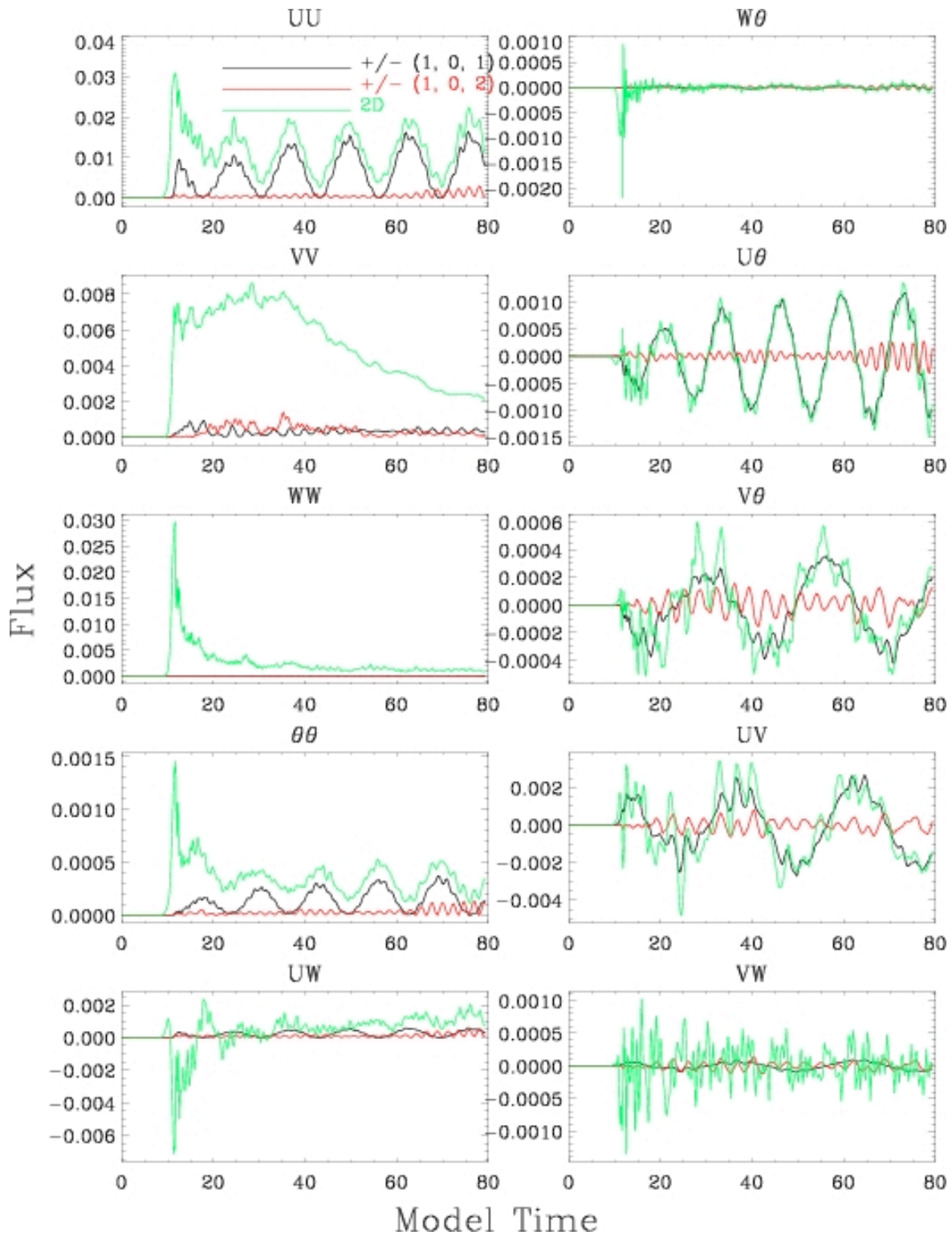


Figure 8. As in Figure 5, but for the two gravest wavenumber pairs having streamwise variations, $\pm(1, 0, 1)$ and $\pm(1, 0, 2)$, shown with black and red lines, respectively. The totals for all 2D motions shown previously in Figure 7 are reproduced as green lines for comparison.

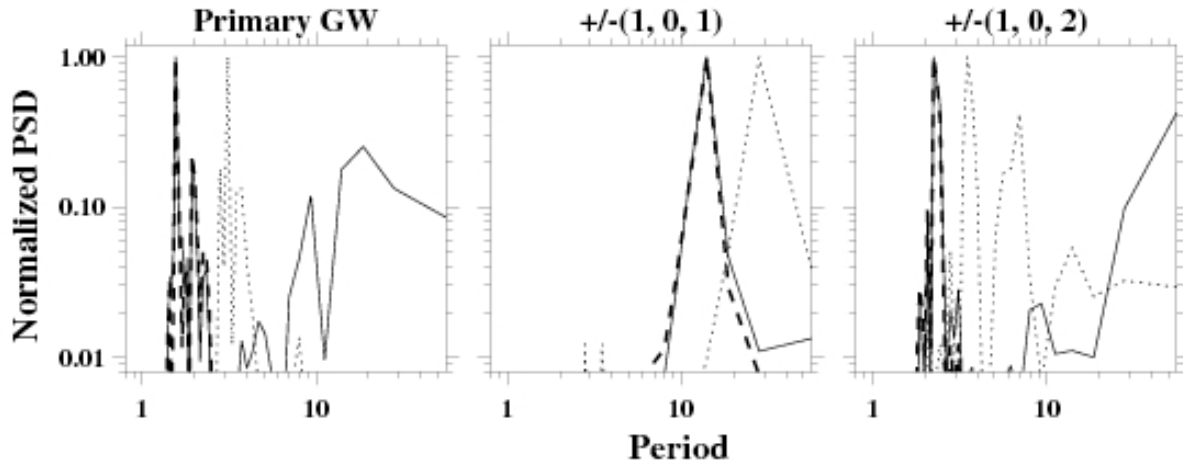


Figure 9. Frequency spectra of the primary GW (left), modes $\pm(1, 0, 1)$ (center), and modes $\pm(1, 0, 2)$ (right). Plotted are normalized (summed) mean variances of u' , w' , and θ' and the streamwise momentum flux (class 1, solid), vertical and streamwise potential temperature fluxes (class 2, long dashed), and momentum and potential temperature fluxes involving v' (class 3, short dashed). All spectra are normalized to 1 at the largest variance or covariance.

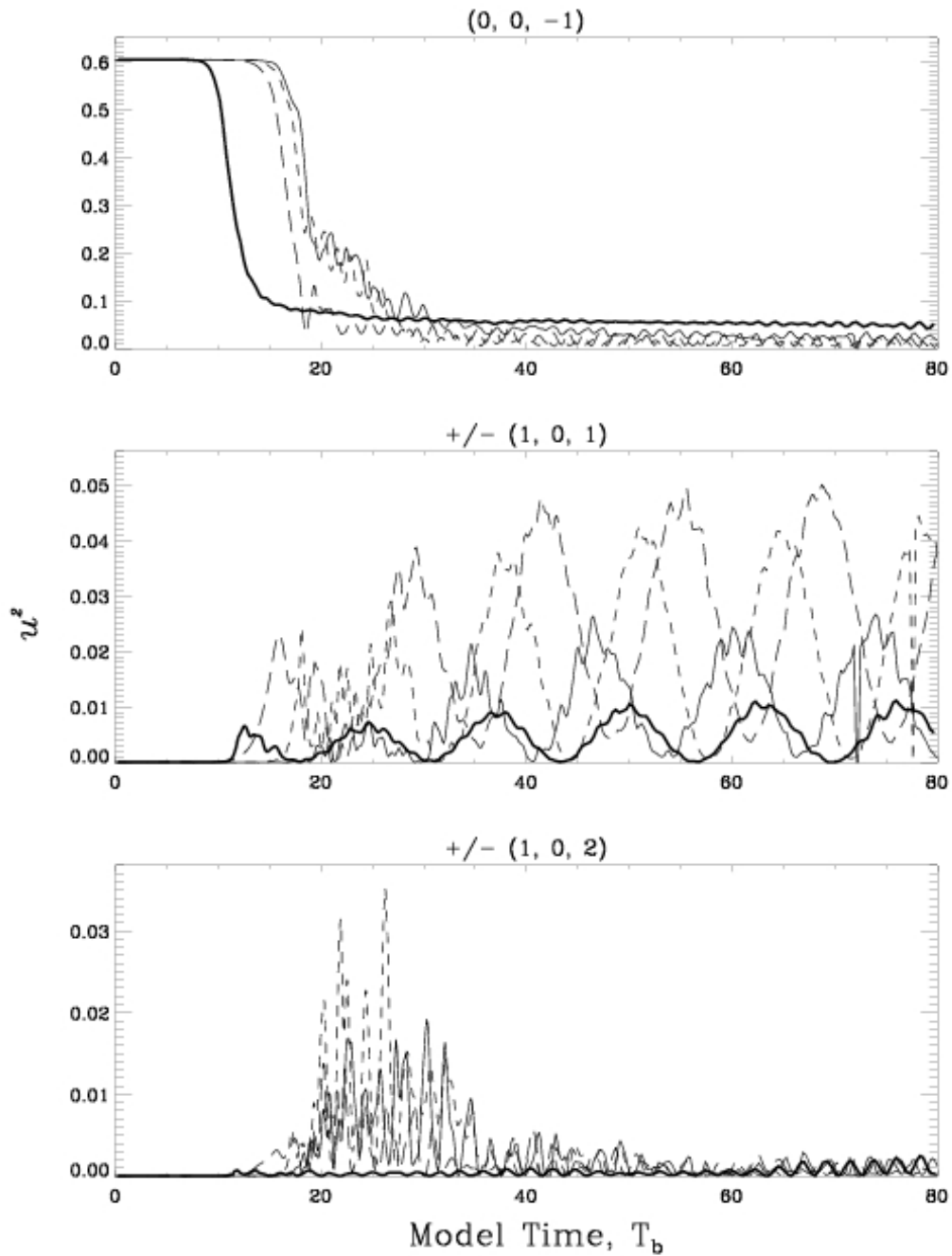


Figure 10. Excitation of the gravest 2D wave modes for $a = 1.1$ by 3D breaking dynamics (heavy solid), and by 2D wave-wave interactions with random initial phase (solid), uniform phase at one streamwise location (long dashed), and the same phase as in the 3D simulation (short dashed). The three panels show the variances of the initial GW with wavenumber $(0,0,-1)$ (top), modes $\pm(1,0,1)$ (middle), and $\pm(1,0,2)$ (bottom).

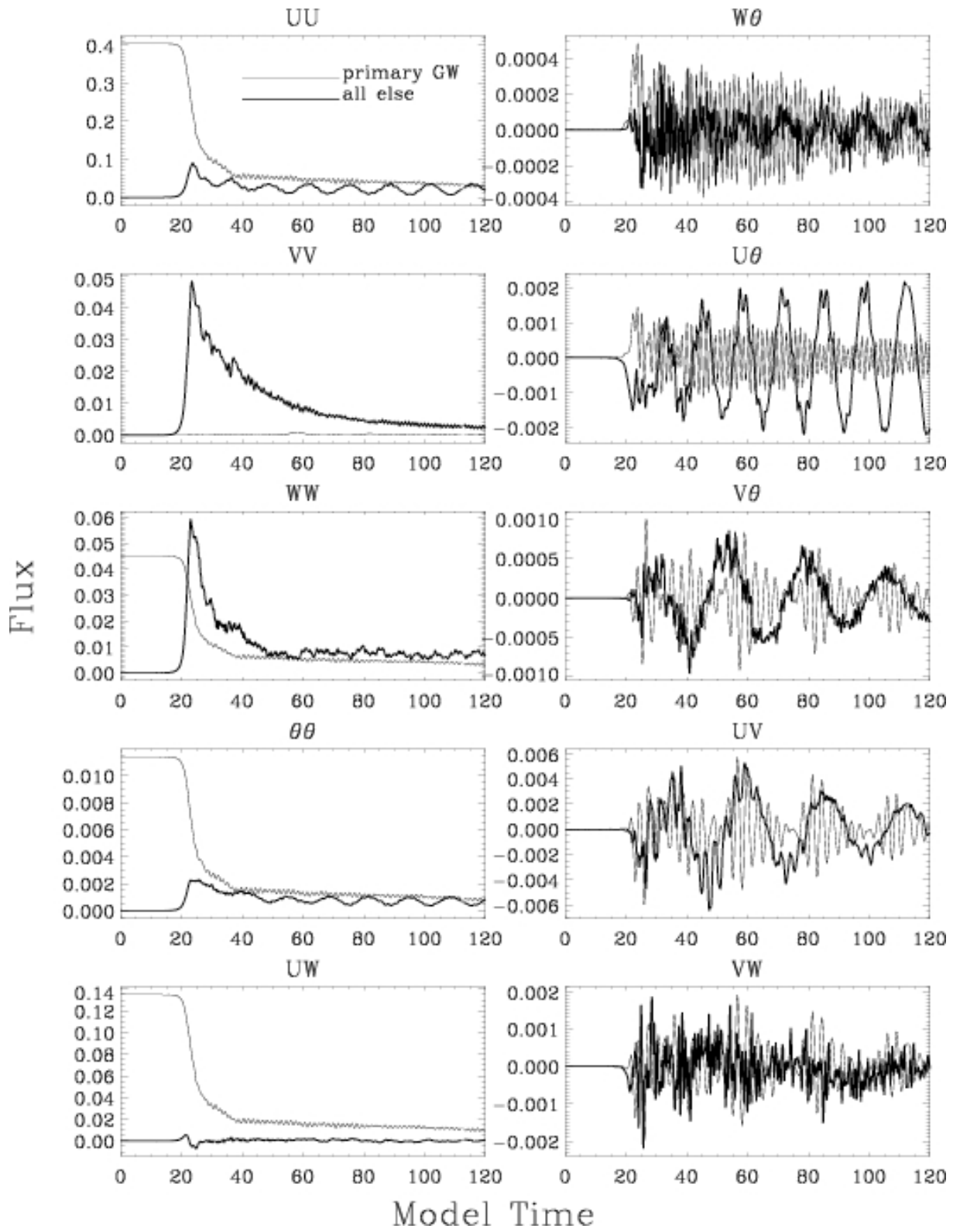


Figure 11. As in Figure 5, but for $a = 0.9$.

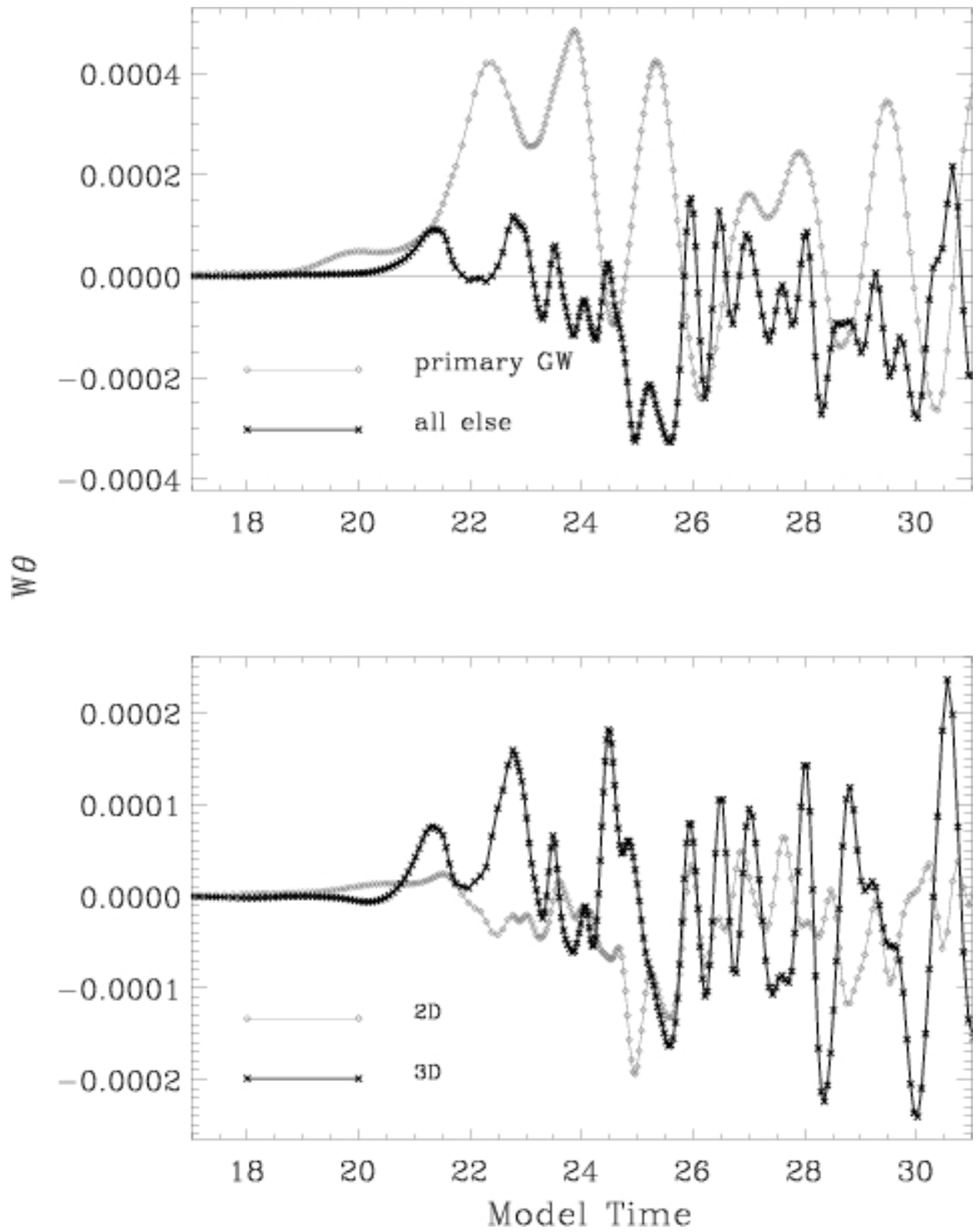


Figure 12. As in Figure 6 but for $a = 0.9$.

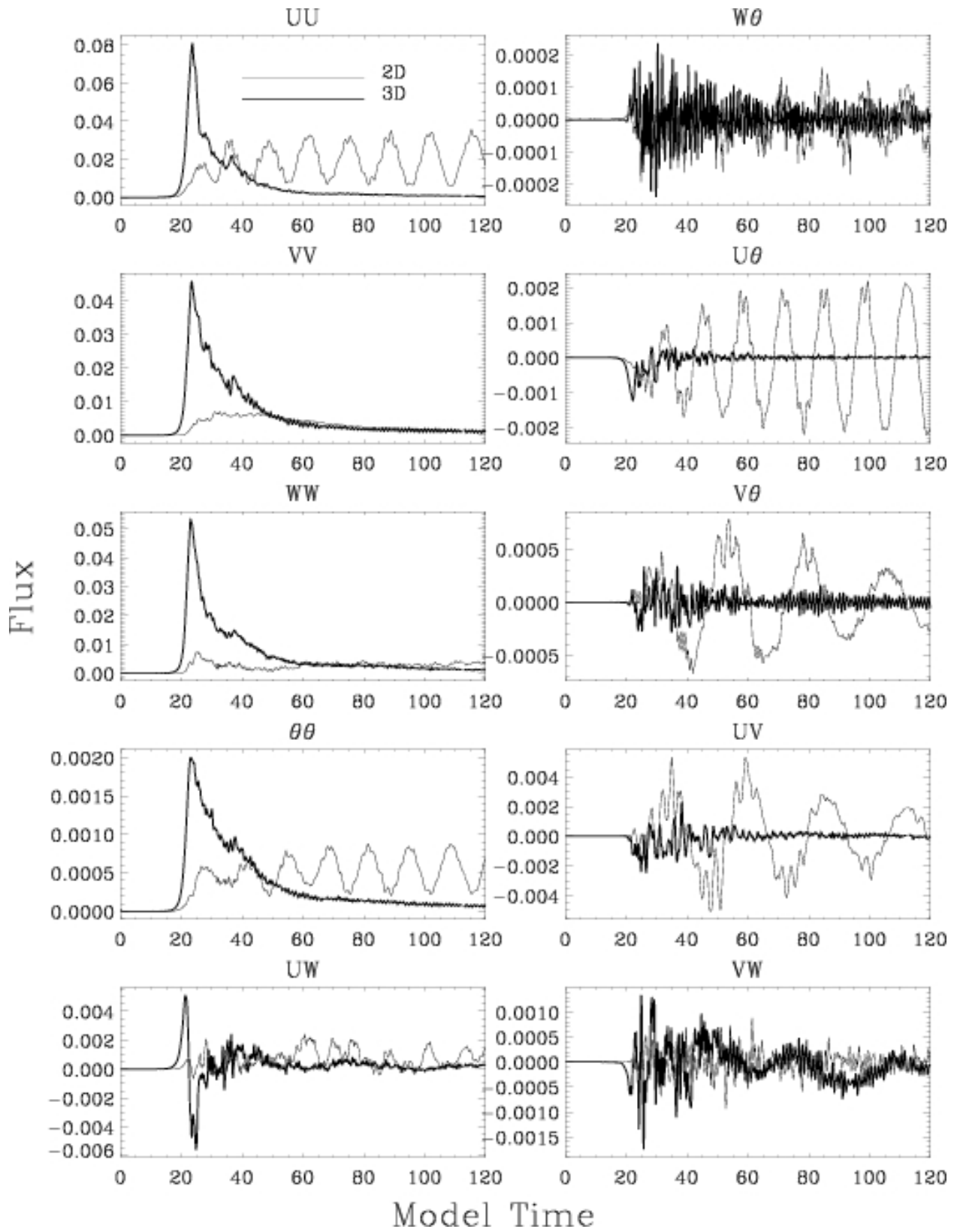


Figure 13. As in Figure 7, but for $a = 0.9$.

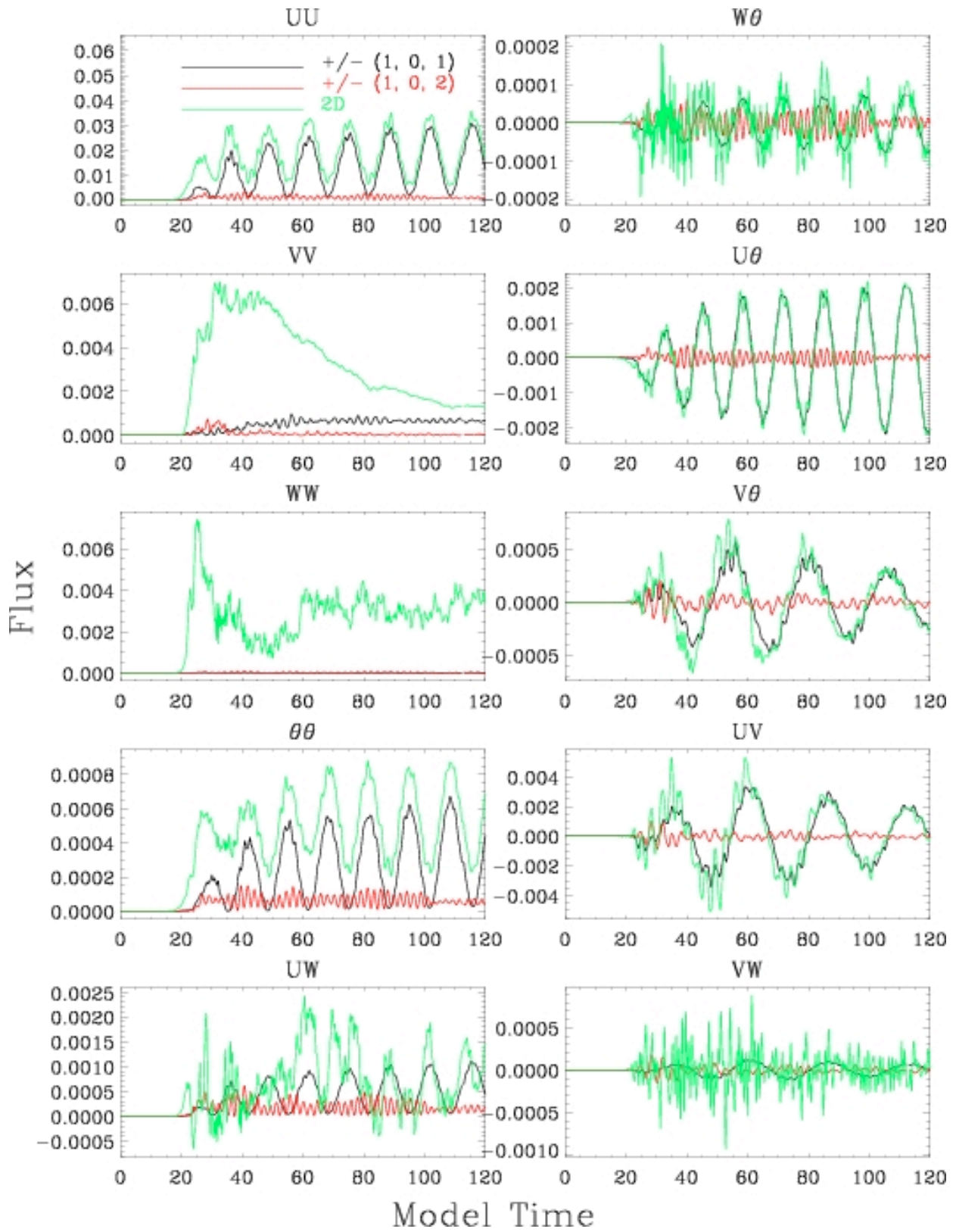


Figure 14. As in Figure 8, but for $a = 0.9$. The totals for all 2D motions shown previously in Figure 10 are reproduced as green lines for comparison.

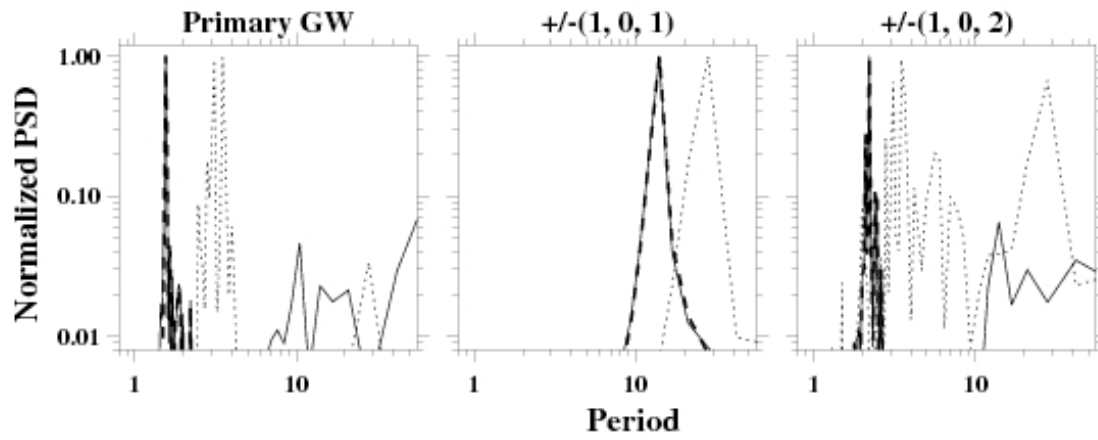


Figure 15. As in Fig. 9, but for $a = 0.9$. In this case, spectra were computed for times from 36 to 120.

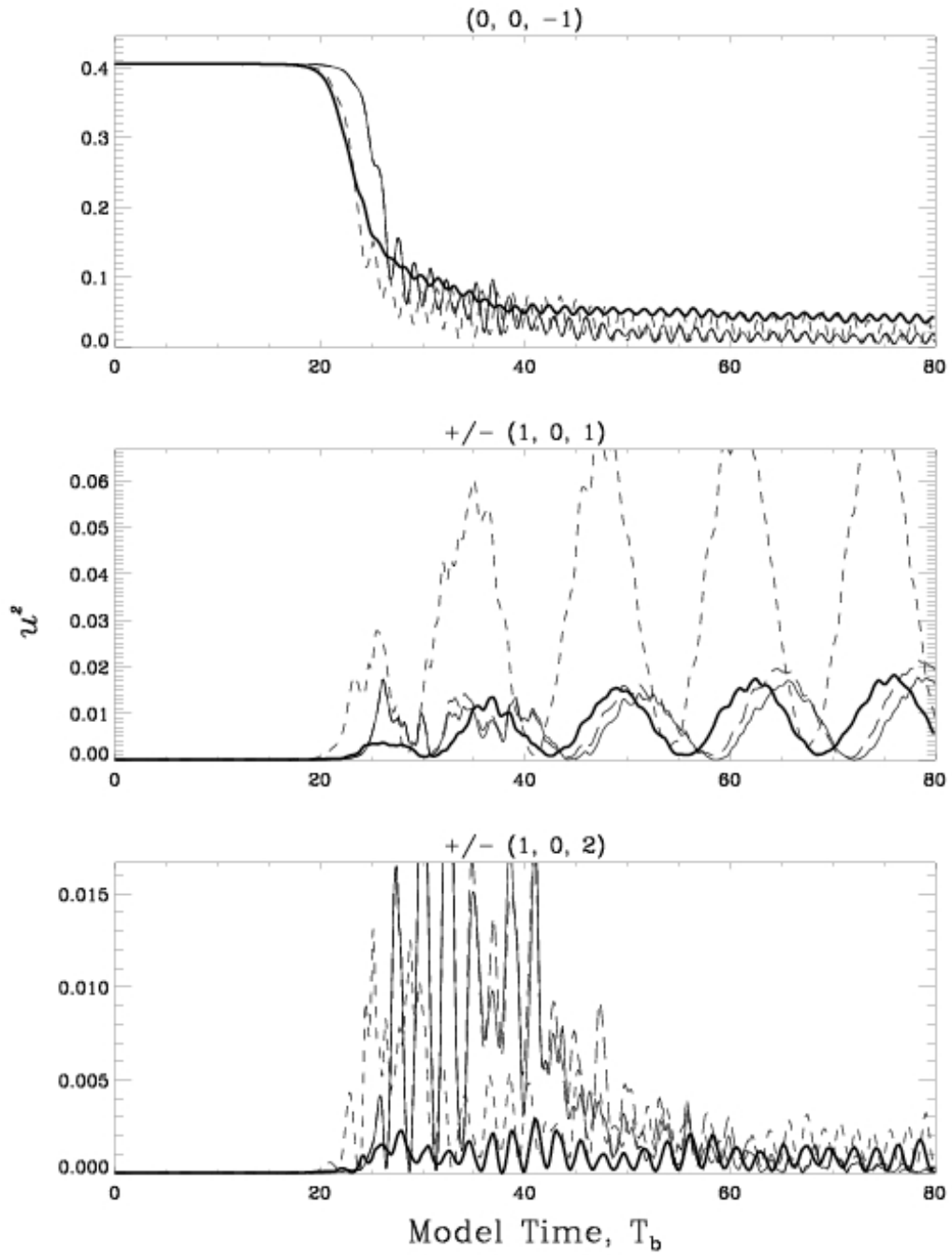


Figure 16. As in Fig. 10, but for $a = 0.9$.